

# Hollow silica nanospheres as thermal insulation materials for construction: Impact of their morphologies as a function of synthesis pathways and starting materials

Ng, S., Jelle, B. P., Sandberg, L. I., Gao, T., & Alex Mofid, S.

Citation for the published version (APA 6th)
Ng, S., Jelle, B. P., Sandberg, L. I., Gao, T., & Alex Mofid, S. (2018). Hollow silica nanospheres as thermal insulation materials for construction: Impact of their morphologies as a function of synthesis pathways and starting materials. Construction and Building Materials, 166, 72-80. doi:https://doi.org/10.1016/j.conbuildmat.2018.01.054

# Hollow Silica Nanospheres as Thermal Insulation Materials for Construction: Impact of their Morphologies as a Function of Synthesis Pathways and Starting Materials

Serina Ng[a], Bjørn Petter Jelle[a,b], Linn Ingunn Sandberg[b], Tao Gao[b] and Sohrab Alex Mofid[b]

[a]SINTEF Building and Infrastructure, Department of Materials and Structures, NO-7465 Trondheim, Norway.

[b]Norwegian University of Science and Technology (NTNU), Department of Civil and Environmental Engineering, NO-7491 Trondheim, Norway.

Corresponding author: serina.ng@sintef.no (email), +47 930 02055 (phone).

Abstract

Hollow silica nanospheres (HSNS) show a promising potential to become good thermal insulators with low thermal conductivity values for construction purposes. The thermal conductivity of HSNSs is dependent on their structural features such as sizes (inner diameter and shell thickness) and shell structures (porous or dense), which are affected by the synthetic methods and procedures including reaction medium, polystyrene template, and silica precursor. . Formation of thermally insulating HSNS was in general favoured by alkaline reaction, whereby highly porous silica shells were formed, promoting less silica per volume of material, thus a lower solid state thermal conductivity. The Knudsen effect is in general reducing the gas thermal conductivity including the gas and pore wall interaction for materials with pore diameters in the nanometer range, which is also valid for our HSNS reported here. Further decreasing the pore sizes would invoke a higher impact from the Knudsen effect. The additional insulating effect of the inter-silica voids (median diameter $D_{50} \approx 15$ nm) within the shell coating contributed also to the insulating properties of HSNS. The synthesis route with tetraethyl orthosilicate

(TEOS) was more robust and produced more porous silica shells than the one with water glass ($Na_2SiO_3$, WG), although the latter might represent a greener synthetic method.

**Keywords:** Hollow silica nanosphere, HSNS, Nano insulation material, NIM, Thermal conductivity, silica, Knudsen effect, porosity, green material.

## 1. Introduction

According to the EU commission, heating and hot water alone accounts for 79% of total final energy use (192.5 Mtoe). While cooling is a fairly small share of total final energy use, demands from households and businesses such as food industry rise during the summer months. Therefore, in order to fulfil the EU's climate and energy goals of more than 20% energy savings by 2050, the heating and cooling sector must sharply reduce its energy consumption.

High-performance thermal insulation materials for buildings is one of the most direct methods to meet the demand of improved energy efficiency. Studies [1] have demonstrated that energy efficiency measures such as thermal insulation retrofit are the most cost-effective with respect to $CO_2$ emissions, whereas other measures e.g. solar photovoltaics and wind energy are far less cost-effective. Today, efforts are being put into moving from the common thermal insulation materials [2] to develop new materials with as low thermal conductivity as possible [3–9]. While this is the best solution for construction purposes, the current state-of-the-art thermal insulation materials are still in their infancy. Further work is needed before proper incorporation into the building industry could be achieved at an affordable cost.

Both macro and micro scale developments have been conducted. The latest trend is to develop nanostructured thermal insulation materials, which can function and thermally insulate from the nano scale. A promising class of nanostructured thermal insulation materials are the nano-hybrid composite consisting of organic/inorganic particles and inorganic hollow particles. These materials have been

investigated extensively in the context of chemistry and materials science. Principally, composite organic/inorganic particles can be classified as organic core with an inorganic shell or vice versa. Both polymer encapsulation of inorganic particles and coating of polymer particles with minerals can modify the properties of the precursor particles and lead to nanocomposite particles with tailored structures and morphologies [10,11]. Considerable research has been devoted to the preparation of mineral-coated polymer particles, and there are three main approaches: sol-gel nano-coating [12–16], hetero-coagulation [17] and layer-by-layer self-assembly [18]. By far, sol-gel synthesis is the most attractive for forming core-shell particles due to its ease of operation. Hollow nanospheres can be produced from hybrid nanoparticles, by extraction of the polymeric core through methods such as calcination, solvation, etc.

Among the different elements, silica is the most abundant chemical compound in the earth crust, most commonly found in nature as quartz and as the major constituent of sand. Its abundancy makes it a logical starting point material on the path to create nano insulation materials (NIM) for the future [19–21]. In parallel, our laboratory has been working on the development of new composite materials involving silica aerogel-concrete hybrids for both structural and thermal insulation properties so as to minimize the thickness of the material during construction [22–25]. Hollow silica nanospheres (HSNS) could potentially be a replacement material for silica aerogels. HSNS could also potentially be a replacement for thermal insulation materials such as expanded polystyrene (EPS) and extruded polystyrene (XPS), materials that may suffer from challenges related to fire, apart from their relatively large thermal conductivity values compared to silica aerogel [7].

This investigation thus aims to analyze the creation of thermally insulating hollow silica nanospheres (HSNS) for construction purposes. The current investigation is a follow-up on our investigations on the formation of HSNS based on a sacrificial polystyrene template and a silica precursor of tetraethyl orthosilicate (TEOS) [19–21]. We have previously shown that through such synthesis methods, thermally insulating materials with low thermal conductivity values of about 20 – 40 mW/(mK)can be produced [20, 26], although the overall carbon footprint may be relatively high due to the use of organic silica precursor. It

was then suggested that water glass ($Na_2SiO_3$, WG) can be an alternative for lowering the carbon footprint. The current investigation will thus explore the alternative synthesis route using water glass as the silica precursor. The synthesis of spherical polystyrene templates and formation of HSNS with TEOS will first be described to form the basis for a water glass based HSNS synthesis. Thereafter, a comparison of the differences in morphological formation of the silica network by applying TEOS and water glass as precursors will be discussed in relation to their thermal conductivity. The parameters affecting the formation, mode of formation and final product will be highlighted.

# 2. Materials and methods

## 2.1. Materials

Reagent grade styrene (St), polyvinvylpyrrolidone (PVP; Mw ≈ 40k Da), potassium sulfate (KPS), ammonium hydroxide ($NH_4OH$, 28~30 wt%), tetraethyl orthosilicate (TEOS), ethanol (96%), water glass (sodium silicate solution, $Na_2SiO_3$, WG) and 1 M hydrochloric acid (HCl) were supplied by Sigma Aldrich.

## 2.2. Synthesis of polystyrene templates

Polystyrene (PS) templates based on varying PVP/St ratios were synthesized via emulsion polymerisation. In a typical synthesis, 10 g of styrene and required amount of PVP were homogenized in 90 g of distilled water at room temperature (RT) for 15 min in a 250 ml Erlenmeyer flask. The following eleven PVP/St ratios were employed: 0.0050, 0.0075, 0.0100, 0.0500, 0.1000, 0.1500, 0.2000, 0.2500, 0.3000, 0.4000 and 0.5000. 0.10 g of KPS dissolved in 10 g of distilled water was then added to the mixture maintained at a constant temperature of 70 ±1°C in an oil bath under stirring conditions of 300 rpm for 24 h before quenching by cooling in air at RT. The PS solutions are denoted as PS-ratio, e.g. PS-0.0050.

## 2.3. Coating PS templates with silica

2.3.1 TEOS as silica precursor

6 g of PS-0.1000 was dispersed in 95 g of 96% ethanol at 500 rpm for 15 min. 1.5 mL of $NH_4OH$ was added (pH was about 13). The mixture was stirred for 15 min. 5 mL of TEOS in 5 mL of ethanol was added to the reacting pot in three manners: (1) TEOS-1: all at once, (2) TEOS-2: 1/5 of the TEOS/ethanol added at hourly interval over a period of 5 h and (3) TEOS-3: 1/100 of TEOS/ethanol added at 3 min interval over 5 h. The final mix was stirred at 500 rpm overnight at RT.

2.3.2 WG as silica precursor

20 g of PS-0.1500 (or PS-0.3000) were mixed with 3 g of WG in 240 g of distilled water. When further PS with lower PVP/St ratios were employed, no stable colloid could be formed at the original PS concentration. For synthesis purposes, an optimized diluted system was employed. To PS-0.0050 and PS-0.0075 samples, 5 g of PS was added to 1 g of WG in 50 g of distilled water. 1 M HCl was added to all samples until a pH of 2.0 was reached. The solutions were left stirring at 400 rpm overnight at RT.

All coated PS-silica samples were subjected to centrifugation at 8000 rpm for 10 min, air dried overnight and calcined at 500°C for 5 h (heating rate = 5°C/min) to remove the PS core.

## 2.5. Characterization

Microstructures of the obtained materials were analyzed by using a Hitachi S-5500 scanning transmission electron microscope (STEM). Analysis with secondary electrons employed an acceleration voltage of 10 kV and current of 7 μA while 30 kV was used in bright field transmission mode.

The thermal conductivity of unmodified PS-silica samples were determined by employing a Hotdisk Thermal Constants Analyzer (TPS 2500S). A transient plane source technique was applied [27, 28] and the PS-silica were measured using the Kapton sensor with radius of 3.189 mm. The sensor is sandwiched between two well packed powder samples of PS-silica . The sensor acts both as a heat source, as well as to register the temperature increase in the samples. The temperature increase over time is recorded and used to calculate the thermal conductivity of the samples. The heating power and heating time can

be varied independently to obtain the most appropriate testing conditions for each sample. The conductivity measurements were performed with a heating power ranging from 100 to 700 mW and a heating time of 320 s. All unmodified PS-silica samples were measured only after cooling to ensure equilibrium of the thermal conductivity. Repacking of the samples for measurements were employed and the final reported data are given as the arithmetic mean of 3 to 5 individual results, depending on the repeatability of the measurements.

# 3. Results and discussion

## 3.1. Size determination of PS templates

A nano insulation material (NIM) is a homogeneous, nanostructured material with closed or open nano-sized pores (**Figure 1**). The overall thermal conductivity ($\lambda_{tot}$) of NIM can be attributed in a simplified form to the proximity of gases to solid interfaces, molecular collisions and the inherent materials properties for heat transfer within a specific area or volume as governed by the following expression:

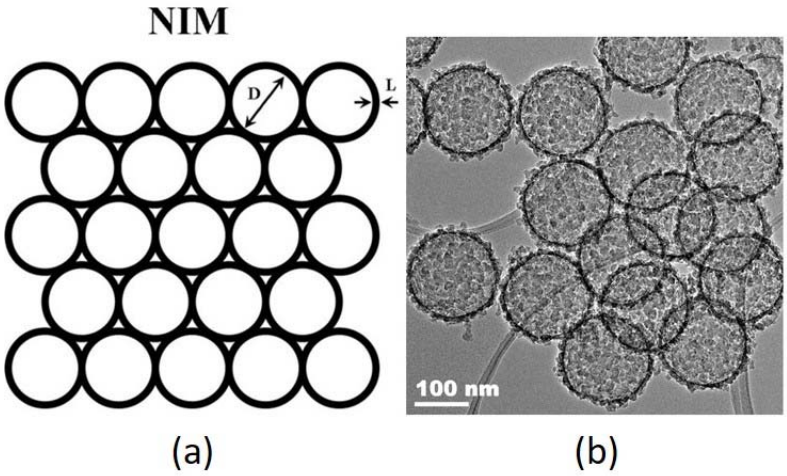


**Figure 1**. (a) Conceptual model of a hollow nanosphere NIM with the pore size D and shell thickness L as dimensional characteristics and (b) TEM image of actual hollow silica nanospheres.

$$\lambda_{tot} = \lambda_{solid} + \lambda_{gas} + \lambda_{rad} + \lambda_{conv} + \lambda_{coupling} \quad \textbf{(1)}$$

where $\lambda_{tot}$ is the total overall thermal conductivity, $\lambda_{solid}$ is the solid state thermal conductivity, $\lambda_{gas}$ is the gas thermal conductivity, $\lambda_{rad}$ is the radiation thermal conductivity, $\lambda_{conv}$ is the convection thermal conductivity, commonly termed as part of the gas thermal conductivity and $\lambda_{coupling}$ is the thermal conductivity term accounting for second order effects between the various thermal conductivities in **Equation 1**. Generally, convection is not an issue in nanostructured thermal insulation materials. The three main determining factors are $\lambda_{solid}$ and $\lambda_{rad}$, which are governed by the material bulk and surface properties, and $\lambda_{gas}$, which is exemplified by the Knudsen effect at nanometer levels [29]. In our investigations, the gas of concern is air at atmospheric pressure, since the air will be entrapped within the HSNS. $\lambda_{gas}$ defined by the Knudsen equation is related to the mean free path of the gas or air molecules and the average diameter of the pores, which further includes the interaction between the gas molecules and the pore walls. It may be written as:

$$\lambda_{gas} = \frac{\lambda_{gas,0}}{1+2\beta Kn} \quad (2)$$

$$Kn = \frac{\sigma_{mean}}{\delta} = \frac{k_B T}{\sqrt{2}\pi d^2 \rho \delta} \quad (3)$$

where $\lambda_{gas}$ is the thermal conductivity of the gas inside the nano-sized pores (also including gas and pore wall interaction); $\lambda_{gas,0}$ is the thermal conductivity of the gas at standard temperature and pressure (STP); $\beta$ is the energy transfer (in)efficiency of the molecule-wall collisions (a unitless number between 1.5 and 2.0); Kn is the Knudsen number; $\sigma_{mean}$ is the mean free path of the gas molecules; $\delta$ is the characteristic pore size of the material; d is the collision diameter of the gas molecules; p is the gas pressure inside the pores; $k_B$ is the Boltzmann's constant; and T is the temperature. It should be noted that when the pores in a material are reduced to matter of nanometers, the Knudsen number becomes very large, which will result in a gas thermal conductivity that approaches zero. As the distance between the pore walls becomes small relative to the mean free path of the gas molecules, it becomes increasingly likely for the molecules to not hit other molecules before colliding with the pore walls, thus reducing the gas thermal conductivity, also including gas and pore wall interaction, within the pores substantially. Therefore, to ensure an effective Knudsen effect and very low thermal conductivity, controlling the size

of PS templates (which influences the eventual length of flow space for air molecules in the insulator) would be a main criteria in determining the thermal conductivity values of HSNS. It has been calculated that the mean free path of ambient air is 68 nm [30], thus the Knudsen effect will be very large when the pore diameter is less than that. As a result, a pore size smaller than or in the range of 68 nm as determined by the smaller diameter of the PS template particles in the nanometer range, is desired in order to achieve a theoretically low thermal conductivity, assuming all other factors are constant.

Similar to other investigations [31], PVP was found to be the most important factor in determining the size of the PS particles, and in affecting the successful synthesis of PS/$SiO_2$ core-shell particles. The stabilizing and surfactant effect of PVP allow size control of the growing PS, resulting in uniformly distributed PS to be synthesized as a function of the PVP/St ratio. In the absence of PVP, PS particles of varying sizes (spherical to oblong) with high polydispersity and diameters up to micro-meters were formed, showing susceptibility to slight variations in KPS and temperature during polymerisation. Upon the addition of PVP, the reaction stabilized and monodispersed PS particles with size dependency on PVP content was attained (**Figure 2a**). The mean particle size distributions of the PS particles were calculated from the SEM images by averaging over hundreds of particles. It was found that the median particle diameter ($D_{50}$) of the PS particles decreased with increasing PVP amounts from 904 ±17 nm at a PVP/St ratio of 0.0050 till an optimal PVP/St ratio of 0.1500 with a $D_{50}$ of 180 ±1 nm (**Figure 2b**). The growth profile of the PS particles can be attributed to the stabilizing effect of the surfactant PVP on styrene, whereby incorporation of PVP on the surfaces of the PS particles mask the negative charges of the pi bonds of St, hence preventing propagation of polymerisation.

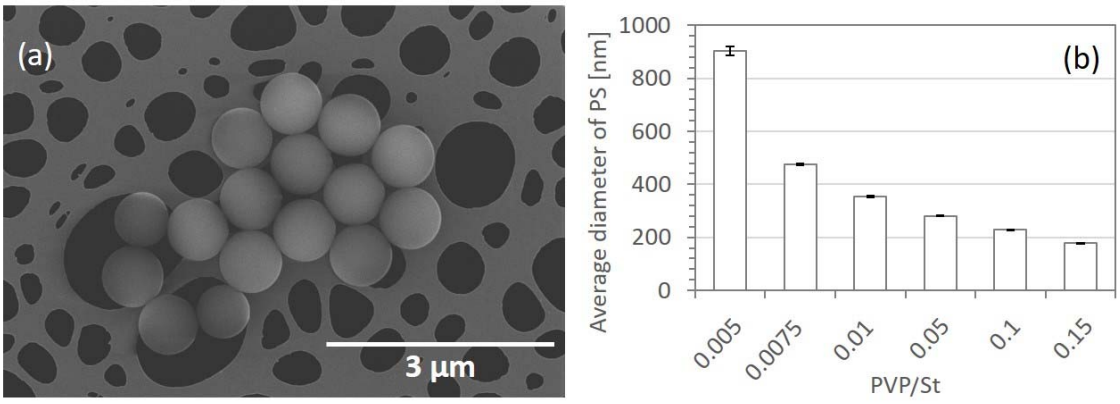


**Figure 2**. (a) SEM images displaying monodisperse PS particles prepared with a PVP/St ratio of 0.0050, (b) $D_{50}$ of PS particles as a function of PVP/St.

Further increase in PVP/St up to a ratio of 0.3000 resulted in the formation of bimodal PS particles (**Figure 3**). The samples prepared at a PVP/St ratio of 0.3000 displayed a bimodal particle size distribution, with respective $D_{50}$ of PS particles in the samples at approximately 450 µm and 120 µm. At PVP/St ratios of 0.4000 and 0.5000, no PS particles were detected, potentially due to the over-dispersing effectiveness of PVP on St, which increased the surface tension of PS particles and prevented the formation of spherical particles. For subsequent studies, PS-0.1500 and PS-0.1000 with an average diameter of ~200 nm, were mainly chosen for templating due to their sizes and stability in their respective mediums.

The $D_{50}$ of PS templates for subsequent employment signified a diminishing Knudsen effect in the HSNS in our investigations.

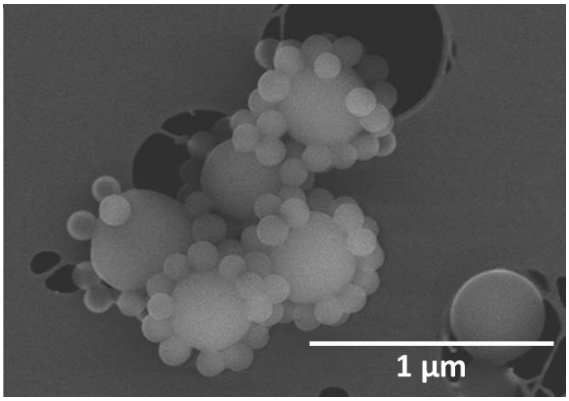


**Figure 3**. SEM image displaying PS particles prepared at a PVP/St ratio of 0.3000.

The amphiphilic characteristic of PVP arising from the presence of the highly polar amide group within the pyrrolidone ring, polar methylene and methine groups in the ring [32, 33] and along the backbone, allow modification of the PS surfaces to increase interfacial coupling with silica monomers or oligomers. Therefore, PS particles were subjected to direct coating with silica precursors through a modified Stöber process. A total of three different TEOS systems and one with WG were employed. The choice of WG can be boiled down mainly to the environmental friendliness of this material, where the medium was water. In the case of TEOS, ethanol was employed.

### 3.2. TEOS as silica precursor

Coating of PS-0.1000 under alkaline conditions by using TEOS as silica precursor was successful in all cases, and showed high repeatability and robustness in their formations. Nanospheres of ~270 nm were formed, showing a raspberry-like morphology. After calcination, all samples maintained the raspberry-like appearance with an average particle size of ~250 nm and appeared as monodispersed globules of consolidated silica nanoparticles. Under TEM imaging, these nanospheres/nanoclusters were hollow, confirming that the PS template had been successfully removed during calcination (**Figure 4**, right).

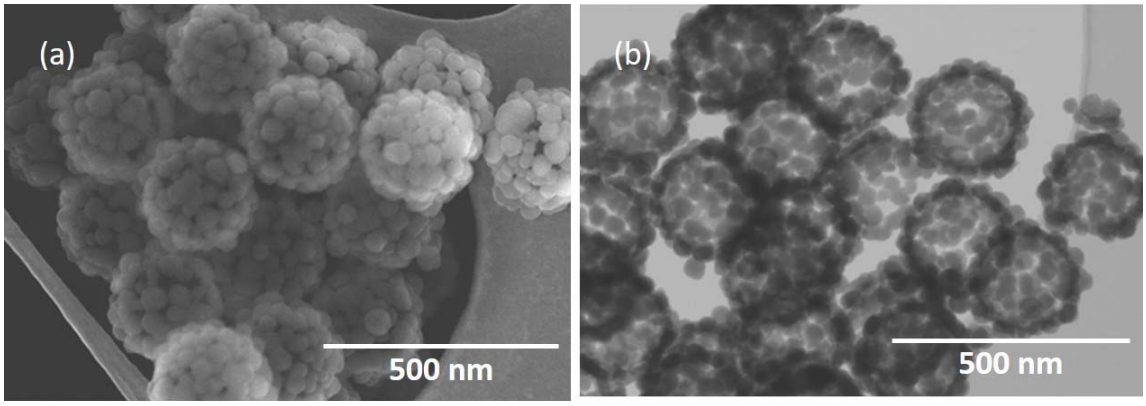


**Figure 4**. HSNS prepared from PS-0.1000 and TEOS-1 after calcination (a) SEM image (b) TEM image.

The inner diameter of the globular particle was ~200 nm, 10% smaller than the original PS template indicating a coalescing effect of the silica nanoparticles upon calcination. This causes the loosely bound silica nanoparticles to be knitted more closely together. From the TEM image (**Figure 4b**), it can be observed that gaps can still be observed between individual silica nanoparticles within each coating, indicating a highly porous shell structure. The thickness of the silica shell was approximately 50 nm in width (**Figure 5a**). Each individual silica nanoparticle was dense and had a $D_{50}$ of ~30 nm, independent of rate at which TEOS was added (**Figure 5b**). This signified that a mono- to bilayer of silica nanoparticles was formed around the PS template during the coating process. The formation of individual silica nanoparticles may be attributed to the formation of highly branched discrete silicate oligomer species under alkaline conditions. The shapes and sizes of final products (solid core and hollow silica nanospheres) were independent of the mode of TEOS/ethanol addition, implying that the synthesis route of the silica monomers is more dependent on the size of the PS templates, surface tension of the forming silica nanoparticles and their interaction with the medium, than on kinetic parameters or conditions, indicating a robust formation pathway.

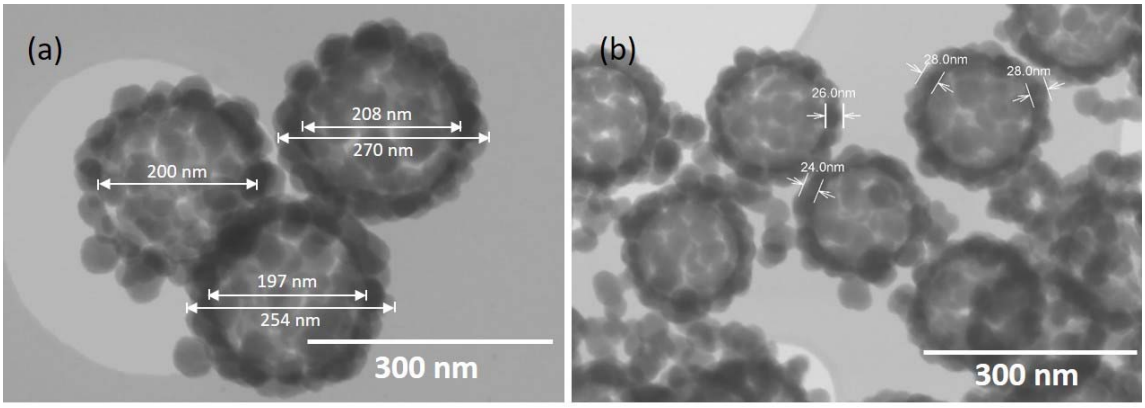


**Figure 5**. Measured nanosilica globules prepared from PS-0.1000 and TEOS–1, demonstrating by measurement bars the (a) inner and outer circumferences and (b) size of individual silica particles.

For determining the robustness of the synthesis route, a further experiment was performed to deduce the effect of the medium, i.e. addition of water on the hydrolysis rate of TEOS in forming the hollow nanospheres. It is known from literature that up to a threshold limit, increase in water content will favour hydrolysis of TEOS and gelation of silica [34]. In our investigations, when the purity of ethanol was altered from 96% to 100%, smaller silica nanoparticles of ~5% reduction in size were observed in the latter, indicating that despite the apparent effect of the hydrolytic consequence of water on the system, the overall medium dominated by the pH remains as the main determining factor in the formation of silica particles.

### 3.3. WG as silica precursor

Due to the low reactivity of water glass (WG), it was employed as a silica precursor at a low pH of about 2. This specific acidic condition was employed to promote electrostatic deposition onto PS as silica nanoparticles are positively charged below this isoelectric point [35]. Successfully coating of PS-0.1500 with WG depicts a rough, continuous layer of amorphous silica deposit after synthesis and initial air cooling (**Figure 6**). This process of air drying was necessary to stabilize and retain the morphology of the silica structure. However, unlike its counter TEOS based formulation, by-products were often exhibited, such as silica rods (**Figure 7)**. The occurrence of these by-products increases proportionally as the amount of added HCl decreases, suggesting the electrostatic buffering effect of the PVP on the

surfaces of PS particles, which suppressed the overall negative charge of the surfaces of PS particles. Further research efforts are obviously required to optimize the synthetic conditions to achieve better silica coatings from the WG system.

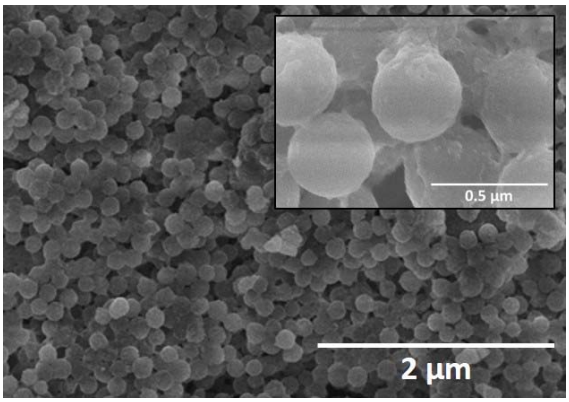


**Figure 6**. Silica coated PS-0.1500 samples from water glass at pH =2.0.

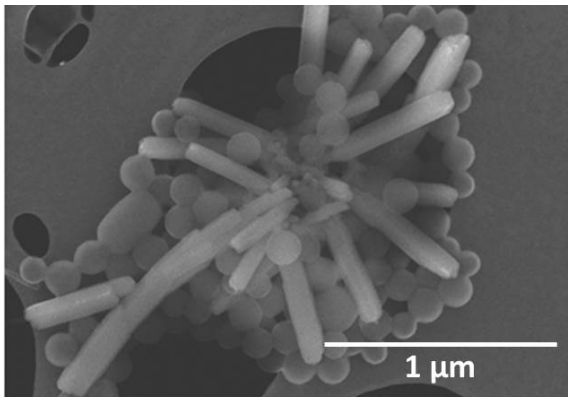


**Figure 7**. By-products from WG-PS-0.1500 silica rods and non-reacted PS particles.

To verify the viability of WG as a silica precursor without the negative impact from PVP, further experiments were conducted with PS-0.0050 and PS-0.0075. According to extrapolation of values from Zou et al. [31], the amount of PVP exposed on the surfaces of PS particles would be less than 1% and 3% for PS-0.0050 and PS-0.0075, respectively (versus 25% for PS-0.1500). This renders the buffering effect of the PVP molecules to be insufficient to mask the negative charges on the PS particles arising from the sulphate groups. In this way, electrostatic attraction between PS and silica under acidic

conditions can be promoted [36]. Samples containing WG and PS-0.0075 showed a blend of coated and non-coated (PS templates that are not successfully coated by silica during reaction) samples. The average diameter of the coated samples was between 500 nm to 600 nm (**Figure 8**).

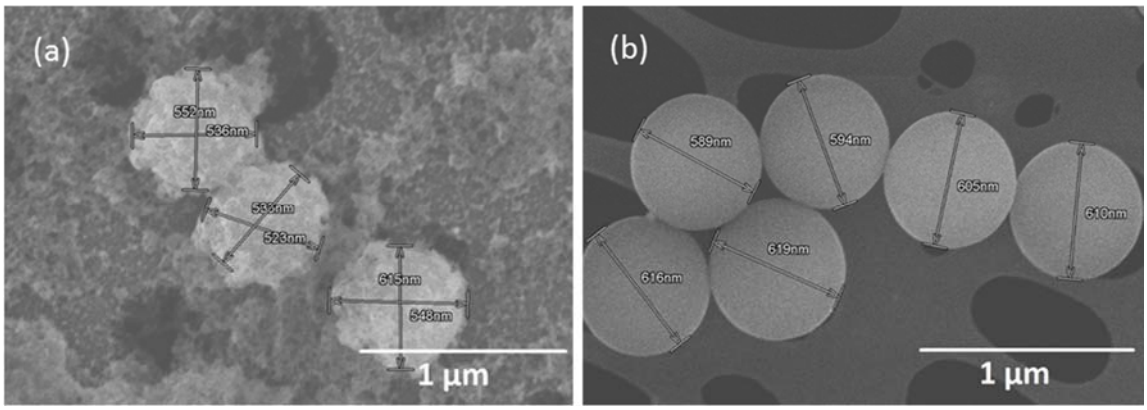


**Figure 8**. PS-0.0075 (a) coated and (b) non-coated with silica from water glass, pH =2.0.

On the other hand, successful full coating of PS-0.0050 was observed. Particles with average diameters of between 600 to 1000 nm were produced (**Figure 9a**), implying the instability of the synthesis route, particularly when using these PS templates. The larger particles could potentially be formed due to coalescing of smaller PS particles together due to low amount of PVP stabilizer. On the other hand, smaller WG-PS particles are created in the same manner as the previous PS-WG hybrid, with shrinkage as a result of calcination. At higher magnifications, the surfaces of the resulting particles were unlike the silica shells of the TEOS based nanospheres, but resembled a large, continuous wrinkled sheet (**Figure 9b**). This may be explained by the tendency of polymerization to undergo slow hydrolysis at low pH, whereby the silica tends to form linear molecules that are occasionally cross-linked. These molecular chains can in turn entangle and form additional branches resulting in gelation and formation of a continuous layer, as amplified by **Figure 9**.

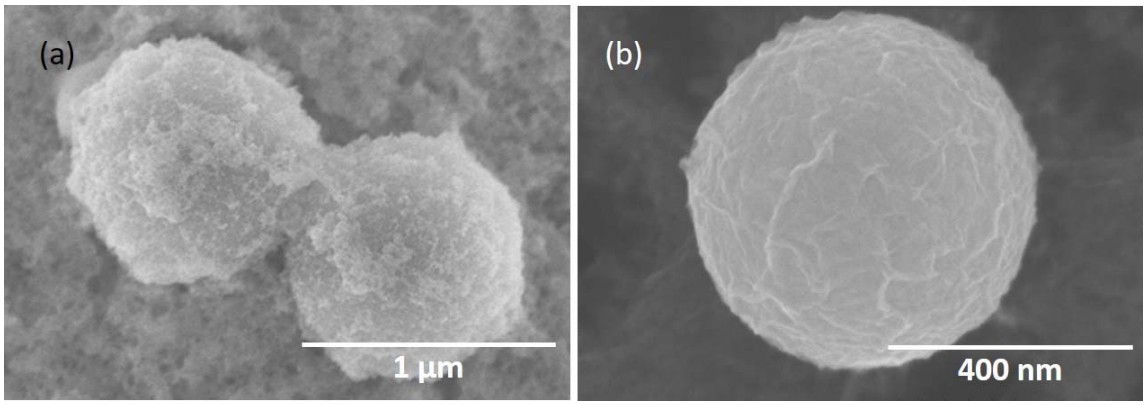


**Figure 9**. (a) PS-0.0050 coated with silica from water glass pH= 2.0. (b) Appearance of the silica shell when coated by WG PS-0.005

On the other extreme, PS-0.3000 samples were coated with WG in a similar fashion as the former three samples and by-products of silica rods were found in higher amounts than that in PS-0.15000 scattered in the sample. While not all PS templates were coated, similar forms of continuous layers of silica coatings on the PS particles were observed. In such cases, the average particle sizes of coated samples were smaller than when PS-0.1500 was employed, standing at a value of ~150 nm. The larger PS on the other hand, were mostly non-coated (**Figure 10**).

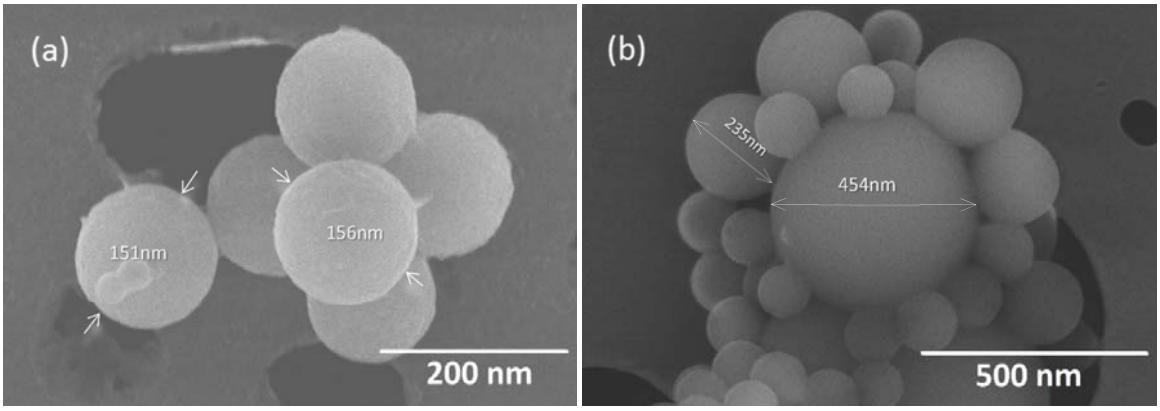


**Figure 10** (a) Coated PS-0.3000 particles and (b) non-coated PS-0.3000 particles in the presence of WG.

Upon calcination, compact mass clusters of nanospheres were detected. For samples prepared with PS-0.1500, the average $D_{50}$ was ~120 nm (**Figure 11**). Two points could be observed here. Firstly, not all PS from coated particles were successfully removed through calcination, potentially due to the impermeable continuous layer of silica deposit on the PS particles (**Figure 9**). However, non-coated PS appeared to be removed during calcination. Secondly, the WG-PS particles were much smaller than the PS-0.1500 precursor (120 nm versus 180 nm, respectively), signifying a reduction of up to 35% in inner core space of the HSNS during calcination. A similar trend was observed for the other WG-PS samples. Higher magnification view of the silica layer displayed that no separation between single silica particles could be detected. Instead, a single continuous layer of between 10 to 20nm of silica network could be detected (**Figure 12**), approximately half to one-third the width of that from the TEOS systems.

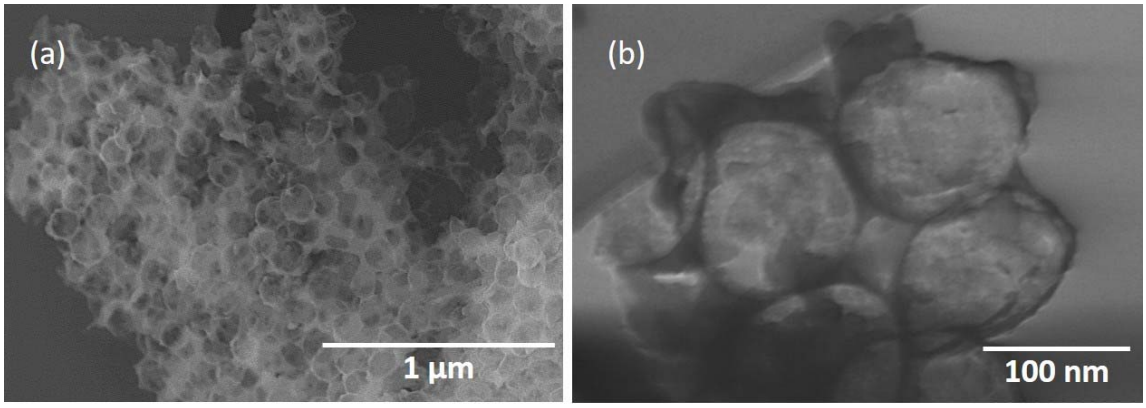


**Figure 11**. Hollow WG based PS-0.1500 samples after calcination, pH=2.0.

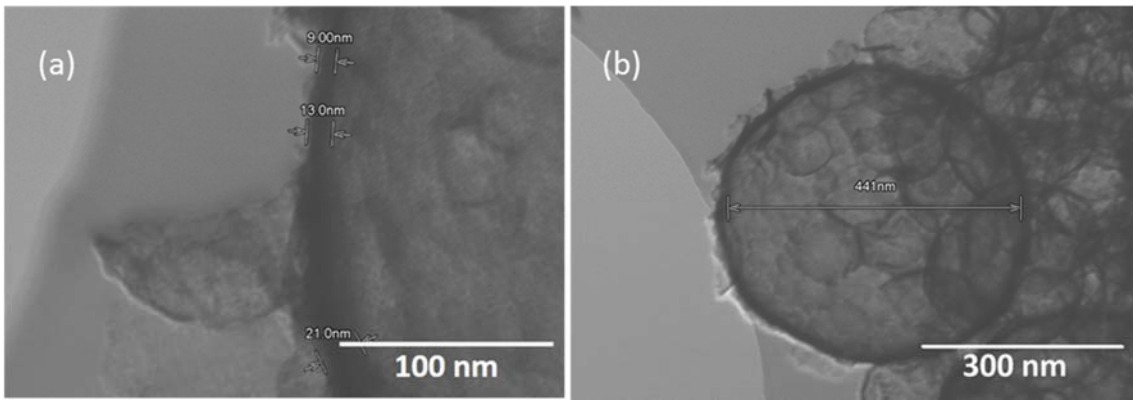


**Figure 12**. (a) Shell thickness of silica layer (between 10 to 20 nm) and measured inner diameter of HSNS prepared with WG and PS-0.1500 (b) lower magnification of same sample.

### 3.4. Thermal conductivity of HSNS

**Table 1** presents the thermal conductivities of the samples prepared from the TEOS and WG reaction systems. All samples were measured directly after calcination without further processing. Compared to the parent material of silica that possessed a thermal conductivity of ~1400 mW/(mK), the prepared HSNS were much lower in thermal conductivity.

**Table 1**. Thermal conductivities of HSNS and their corresponding median particle diameter ($D_{50}$) values (before and after coating).

| No. | Sample name | Thermal conductivity [mW/(mK)] | $D_{50\ avg}$ [nm] | | |
|---|---|---|---|---|---|
| | | | PS only | Coated | Inner D^ |
| 1 | TEOS-1PS-0.1000 (96% EtOH) | 46 | 220 | 250 | 200 |
| 2 | TEOS-2PS-0.1000 (96% EtOH) | 45 | 220 | 250 | 200 |
| 3 | TEOS-3PS-0.1000 (96% EtOH) | 45 | 220 | 250 | 200 |
| 4 | TEOS-1PS-0.1000 (100% EtOH) | 48 | 220 | 245 | 195 |
| 5 | WG-PS-0.3000* | 72 | 160** | 150** | 135 |
| 6 | WG-PS-0.1500* | 102 | 180 | 120 | 105 |
| 7 | WG-PS-0.0075 | 56 | 500 | Varied*** | - |
| 8 | WG-PS-0.0050 | 44 | 900 | Varied*** | - |

*Presence of non-reacted silica rods dispersed within sample: WG-PS-0.3000 > WG-PS-0.15000.

**Only the smaller PS particles were taken into account here and measurements for coated samples are taken before calcination. Most of the large PS particles remained non-coated and were burnt off during calcination.

***Particle sizes varied between 400 to 1000 nm.

^Estimated inner diameter based on silica layer thickness and final coated HSNS $D_{50}$ values

All samples prepared with TEOS displayed thermal conductivity values of between 45 to 48 mW/(mK), which are much higher than the previously reported values [37]. This variation can be attributed to experimental uncertainties like e.g. variation in sample packing density during measurement, which can cause disturbances in the measured thermal conductivity. The consistent thermal conductivity values of TEOS prepared HSNS signified that slight variations in particle size and mode of formation did not affect the thermal conductivity of the final product.

Comparing the TEOS and WG formed HSNS, the reaction medium played a crucial role in determining the nature of the silica particles formed. When WG was employed, the thermal conductivity of the resulting products varied as a function of the PVP/St ratio of the PS templates, whereby the lowest thermal conductivity was registered for samples prepared with PS-0.0050 before attaining a maximum of 102 mW/(mK) with PS-0.1500, and finally stabilizing at 72 mW/(mK) for PS-0.3000. At first glance, it appeared that the variation in thermal conductivity was reversely proportional to the size of particles, which would act against the Knudsen effect, or in a broader sense the overall gas thermal conductivity. However, as observed in Equation 1, the overall thermal conductivity is a function of many different parameters. The inverse trend may be explained by the amount of WG added at the onset of reaction. About 33% more WG was added to PS-0.1500 and PS-0.3000 as compared to PS-0.0075 and PS-0.0050. Therefore, a plausible explanation could be that the higher thermal conductivities were a result of the higher solid state conductivity. Additionally, the variation in packing sizes and densities for WG-PS-0.1500, WG-PS-0.0075 and WG-PS-0.3000 would cause slight variations among the samples.

The main discrepancy however, arose from the difference in thermal conductivity values between WG-PS-0.15000 and TEOS-PS samples. While TEOS based HSNS were twice as large in dimensions as the WG-PS based samples, the thermal conductivity was, however halved. This apparent discrepancy to the theory based on the gas thermal conductivity may be explained by the presence of inter-particle spaces between the silica nanospheres present in TEOS based HSNS (**Figure 13a**), which were absent in the WG based samples (**Figure 13b**). By assuming a close packing network of identically sized silica nanospheres, the average mass density of the silica nanoparticle layer made from the alkaline reaction with TEOS was ideally at a maximum fraction of 0.74 relative to total volume of the sample, regardless of the size of the particles. This implied that in reality, due to the porous nature of the silica layer from the TEOS synthesis, more than 25% of the TEOS based silica coating was made up of nanopores filled with air, bearing average lengths (pitch $z$) of ~15 nm. In this way, the coagulation of silica nanospheres to form the walls of the TEOS based HSNS resulted in an effective reduction of silica mass per volume of material and at the same time, increased the porosity (amount of air voids) within the sample. These two variations would cause a lower $\lambda_{solid}$ and $\lambda_{gas}$ for the TEOS based samples as compared to the WG

based ones. The large number of nanopores with diameter less than the average mean free path of ambient air molecules (i.e. 68 nm) favored Knudsen effect and can effectively act as buffers for heat transfer, which further compensated for the difference in sizes between TEOS and WG based HSNS (HSNS core diameters: TEOS based 200 nm versus WG based 100 nm). In addition, a continuous connectivity existed between silica particles in the WG based HSNS, which was greatly minimized in the disconnected individually formed silica particles of the TEOS based HSNS. Due to the difference in morphological connectivity, the transmission of heat through the silica solid phase of WG based HSNS was more prevalent than that for TEOS based HSNS.

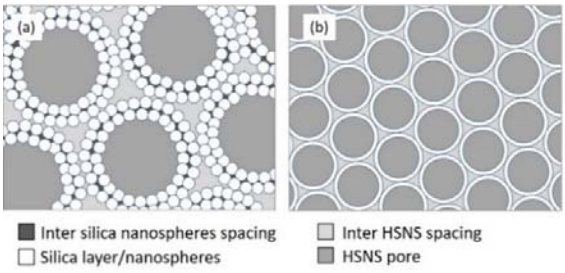


**Figure 13**. Illustration of existing interspacing for the different HSNS samples based on (a) TEOS and (b) WG precursors. Close packing lattices for both systems are assumed (down to scale).

In this way, the overall thermal conductivity of the HSNS was a balance between the $\lambda_{solid}$ of the amount of silica particles, the $\lambda_{solid}$ of the heat transfer based on solid state connectivity and the overall gas conductivity $\lambda_{gas}$, which was governed by the $\lambda_{gas}$ in the HSNS pores, the $\lambda_{gas}$ in the intra-silica layer (HSNS shell) and the $\lambda_{gas}$ in the inter-HSNS. Thus, the net thermal conductivity of WG based HSNS was as a result, higher than that of TEOS based HSNS. In the case of WG-PS-0.0075 and WG-PS-0.0050, no predictable explanations could be given due to the irregularity in the HSNS formed.

In general, the importance of the gas conductivity and the solid state and gas interaction as given by the Knudsen effect should not be downplayed as it plays a major role in the attempts to make the new superinsulation materials of tomorrow. Also note as stated by Kalnæs and Jelle [35] regarding vacuum insulation panels (VIP): "In the case of panel perforation, fumed silica will still have a rather low thermal

conductivity of around 0.020 W/(mK) at atmospheric pressure. Note then that the difference between 0.004 W/(mK) (pristine condition) and 0.020 W/(mK) (punctured) of 0.016 W/(mK) is due entirely to gas thermal conductivity (not taking into account any changes to the solid core due to the loss of vacuum). That is, the combined solid state and radiation thermal conductivity of fumed silica is as low as 0.004 W/(mK) or in principle somewhat lower (as there is still a very small concentration of air inside a VIP a small part of the 0.004 W/(mK) value is due to gas conduction). Hence, as it is possible to make materials with such a very low solid state and radiation conductivity, there are rather good opportunities to make a high performance thermal insulation material functioning at atmospheric pressure by lowering the gas thermal conductivity."

## 4. Conclusions

A series of hollow silica nanospheres (HSNS) were synthesized with tetraethyl orthosilicate (TEOS) and water glass ($Na_2SiO_3$, WG) as silica precursors, in alkaline and acidic media, respectively. It was found that the production with TEOS was more robust and provided a lower thermal conductivity than samples prepared by WG due to increased porosity of the samples, which reduced the effective silica amount per volume of sample (and thus solid state thermal conductivity) and gas thermal conductivity. The lowest thermal conductivity of 44 mW/(mK) of the HSNS samples reported within this study falls in the upper range of traditional thermal insulation materials. Further enhancement of the HSNS properties may be achieved by decreasing the size of the sacrificial templates to decrease the gas thermal conductivity as given by the Knudsen effect, thus making the HSNS a possible stepping-stone toward a viable, new thermal insulation material.

It may be inferred from this investigation that the choice of reaction medium is very important for effective production of thermally insulating HSNS. Therefore, for optimal production, deriving a new synthesis route by using WG as silica precursor may be a possible way to achieve a greener and more sustainable cost-effective method to produce HSNS.

## Acknowledgements

This work has been supported by the Research Council of Norway and several partners through ”The Research Centre on Zero Emission Buildings” (ZEB, project no. 193830) and by the Research Council of Norway through the research project ”High-Performance Nano Insulation Materials” (Hi-Per NIM, project no. 250159) within the Nano2021 program. Furthermore, the Research Council of Norway is acknowledged for the support to the "Norwegian Micro- and Nano-Fabrication Facility" (NorFab, project no. 245963/F50).

## References

1. McKinsey, Pathways to a low-carbon economy. Version 2 of the global greenhouse gas abatement cost curve, McKinsey & Company (2009).
2. M.S. Al-Homoud, Performance characteristics and practical applications of common building thermal insulation materials, Building Environ. 40 (2005) 353–366.
3. A.M. Papadopoulos, State of the art in thermal insulation materials and aims for future developments, Ener. Buildings 37 (2005) 77–86.
4. B.P. Jelle, A. Gustavsen, S. Grynning, E. Wegger, E. Sveipe and R. Baetens, Nanotechnology and possibilities for the thermal building insulation materials of tomorrow, Proceedings of the Renewable Energy Research Conference - Renewable Energy Beyond 2020, Trondheim, Norway, 7–8 June (2010).
5. B.P. Jelle, A. Gustavsen and R. Baetens, The path to the high performance thermal building insulation materials and solutions of tomorrow, J. Building Phys. 34 (2010) 99–123.
6. B.P. Jelle, A. Gustavsen and R. Baetens, The high performance thermal building insulation materials and solutions of tomorrow, Proceedings of the Thermal Performance of the Exterior Envelopes of Whole Buildings XI International Conference (Buildings XI), Clearwater Beach, Florida, U.S.A., 5–9 December (2010).
7. B.P. Jelle, B.G. Tilset, S. Jahren, T. Gao and A. Gustavsen, Vacuum and nanotechnologies for the thermal insulation materials of beyond tomorrow – From concept to experimental

486 investigations, Proceedings of the 10th International Vacuum Insulation Symposium (IVIS-X),
487 pp. 171-178, Ottawa, Canada, 15–16 September (2011).
488 8. B.P. Jelle, Traditional, state-of-the-art and future thermal building insulation materials and
489 solutions - Properties, requirements and possibilities, Ener. Buildings 43 (2011) 2549–2563.
490 9. B.P. Jelle, T. Gao, L.I.C. Sandberg, B.G. Tilset, M. Grandcolas and A. Gustavsen, Thermal
491 superinsulation for building applications – From concepts to experimental investigations,
492 Internat. J. Struct. Anal. Design 1 (2014) 43–50.
493 10. F. Caruso, Nanoengineering of Particle surfaces, Adv. Mater. 13 (2001) 11–22.
494 11. G. Kickelbick, L.M. Liz-Marza´n, In Encyclopedia of Nanoscience and Nanotechnology; Nalwa,
495 H. S. Ed.; American Scientific Publishers: Stevenson Ranch, CA 2 (2004) 199–220.
496 12. H. Bamnolker, B. Nitzan, S. Gura, S.J. Margel, New solid and hollow, magnetic and non-
497 magnetic, organic-inorganic monodispersed hybrid microspheres: synthesis and
498 characterisation, Mater. Sci. Lett. 16 (1997) 1412–1415.
499 13. S. Margel, H.U.S. Bamnolker, Process for the preparation of microspheres and microspheres
500 made thereby, Patent 6,103,379 (2000).
501 14. X. Ding, K. Yu, Y. Jiang, Hari-Bala, H. Zhang, Z. Wang, A novel appraoch to the synthesis of
502 hollow silica nanospheres, Mater. Lett. 58 (2004) 3618–3821.
503 15. C. Graf, D.L.J. Vossen, A. Imhof, A. van Blaaderen, A general method to coat colloidal particle
504 with silica, Langmuir 19 (2003) 6693–6700.
505 16. Y. Chen, E. Kang, K. Neoh, A. Greiner, Preparation of hollow silica nanospheres by surface
506 initiated atom transfer radical polymerization on polymer latex templates, Adv. Funct. Mater.
507 15 (2005) 113–117.
508 17. N. Kawahashi, E.J. Matijevic´, Preparation and properties of uniform coated colloidal particles:
509 V. Yittrium basic carbonate on polystyrene latex, Colloid Interface Sci. 138 (1990) 534–542.
510 18. R.A. Caruso, A. Susha, F. Caruso, Multilayered Titania, Silica, and Laponite Nanoparticle
511 coatings on polystyrene colloidal templates and resulting inorganic hollow spheres, Chem.
512 Mater. 13 (2001) 400–409.

513 19. T. Gao, B.P. Jelle, L.I.C. Sandberg, A. Gustavsen, Monodisperse hollow silica nanospheres for
514 nano insulation materials: Synthesis, characterization, and life cycle assessment. ACS Applied
515 Materials and Interfaces, 5 (2013) 761–767.
516 20. T. Gao, L.I.C. Sandberg, B.P. Jelle, Nano Insulation Materials: Synthesis and Life cycle
517 assessment, Procedia CIRP, 15 (2014) 490–495.
518 21. L.I.C. Sandberg, T. Gao, B.P. Jelle, A. Gustavsen, Synthesis of hollow silica nanospheres by
519 sacrificial polystyrene templates for thermal insulation applications, Adv. Mater. Sci. Engineer.
520 (2013).
521 22. T. Gao, B.P. Jelle, A. Gustavsen, S. Jacobsen, Aerogel-Incorporated Concrete: An Experimental
522 Study, Construct. Build. Mater., 52 (2014) 130–136.
523 23. S. Ng, B.P. Jelle, T. Stæhli, Calcined clay as binder for Thermal insulating and structural aerogel
524 incorporated mortar, Cement and Concrete Composites, 72 (2016) 213–221.
525 24. S. Ng, B.P. Jelle, Y.P. Zhen, O. Wallevik, Effect of storage and curing conditions at elevated
526 temperatures on aerogel-incorporated mortar samples based on UHPC recipe, Construction
527 Building Materials, 106 (2016) 640–649.
528 25. S. Ng, B.P. Jelle, L.I. Sandberg, T. Gao, O. Wallevik, Experimental Investigations of Aerogel-
529 Incorporated Ultra-High Performance Concrete, Construction Building Mater., 77 (2015) 307–
530 316.
531 26. R.D. Schlanbusch, B.P. Jelle, L.I.C. Sandberg, S.M. Fufa, T. Gao, Integration of life cycle
532 assessment in the design of hollow silica nanospheres for thermal insulation applications, Building
533 and Environment, 80 (2014) 115–124.
534 27. S.E. Gustafsson, Transient plane source techniques for thermal conductivity and thermal
535 diffusivity measurements of solid materials, Rev. Sci. Instruments, 62 (1991) 797-804.
536 28. D.P. Bentz, Transient plane source measurements of the thermal properties of hydrating cement
537 pastes, Mater. Struct, 40 (2007) 1073-1080.
538 29. S. E. Kalnæs, B. P. Jelle, Vacuum Insulation Panel Products: A State-of-the-Art Review and
539 Future Research Pathways, *Applied Energy*, **116 (2014)** 355–375.

30. S. Jennings, The mean free path in air, Journal of Aerosol Science, 19, 2 (1988) 159–166.

31. H. Zou, S. Wu, Q. Ran, J. Shen, A simple and low-cost method for the preparation of monodisperse hollow silica spheres, J. Phys. Chem. C, 112 (2008) 11623–11629.

32. J.N. Smith, J. Meadows, P.A. Williams, Adsorption of polyvinvylpyrrolidone onto polystyrene latices and the effect on colloid stability, Langmuir 12 (1996) 3773–3778.

33. P. Molyneux, Water-Soluble Synthetic Polymers: Properties and Behaviour; CRC Press Inc.: Boca Raton, FL (1983).

34. M.A. Fardad, Catalysts and the structure of $SiO_2$ sol-gel films, J. Mater. Sci. 35 (2000) 1835–1841.

35. M.C. Fuji, H. Takai, Imabeppu, X. Xu, Synthesis and shell structure design of hollow silica nanoparticles using polyelectrolyte as template, Tunisia-Japan Symposium: R and D of Energy and Material Sciences for Sustainable Society, TJS 2014, 596 (2015).

36. X. Du, L. Yao, J. He, One-pot fabrication of noble-metal nanoparticles that are encapsulated in hollow silica nanospheres: Dual roles of poly(acrylic acid), Chem. - A European J. 18 (2012) 7878–7885.Kalnæs S.E., Jelle B.P., Vacuum insulation panel products: A state-of-the-art review and future research pathways, Applied Energy, 116 (2014) 355-375.

37. Y. Liao, X. Wu, H. Liu, Y. Chen, Thermal conductivity of powder silica hollow spheres, Thermochimica Acta, 526 (2011) 178–184.